Supporting information of

Conformational distortion of the ionomer backbone for reinforcing the catalyst layer under dynamic operation

Chenyang Zheng,[#a] Di Xiao,[#a] Junfeng Zhang,*[ab] Yabiao Pei,[a] Lianqin Wang,[a] Xin Liu,[a] Yan Yin,*[ab] Michael D. Guiver**[ab] and Xianguo Li[c]

[a] State Key Laboratory of Engines, School of Mechanical Engineering, Tianjin University, Tianjin, 300350, China

[b] National Industry-Education Integration Platform of Energy Storage, Tianjin University, Tianjin, 300350, China

[c] Laboratory for Fuel Cell and Green Energy, Department of Mechanical and Mechatronics Engineering, University of Waterloo, Waterloo, Ontario, N2L3G1, Canada

*Corresponding author. E-mail: gosign@tju.edu.cn

*Corresponding author. E-mail: yanyin@tju.edu.cn

**Corresponding author. E-mail: michael.guiver@outlook.com

Details of commercially-supplied membrane used for CL preparation and single cell test

PiperION AEMs (Fuel Cell Store, USA) are manufactured from functionalized poly(aryl piperidinium) polymer. The general chemical structure of the poly(aryl piperidinium) is shown in Fig. S1:

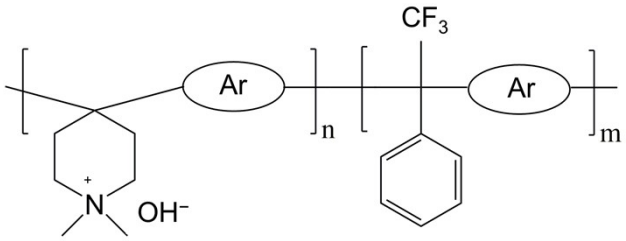

Fig. S1 The general chemical structure of the commercially-supplied PiperION AEMs used for single cell test.

Table S1 Properties of the commercially-supplied PiperION AEMs used for single cell test.

Thickness (μm)	Tensile Strength (MPa)	Young's Modulus	Elongation at Break (%)	IEC (meq g^{-1})	Conductivity OH^- (mS cm^{-1}, 80 °C)
20	>30	>30	>20	~2.35	~150

Comparison of *m*-QAPPT with *p*-QAPPT anion exchange membranes

The properties of the anion exchange membranes *p*-QAPPT and *m*-QAPPT, such as ion exchange capacity, swelling ratio, water absorption ratio, ion conductivity and ionomer viscosity average molecular weight are listed in Table 1. Compared with *m*-QAPPT, the WU of *p*-QAPPT at 80 ℃ increased from 22.90% to 35.91%, and the SR increased from 4.21% to 10.93%. This may be due to the polymer chain folding caused by the more kinked backbone of *m*-QAPPT, as shown in Fig. 3. This renders *m*-QAPPT more compact with less free volume for water absorption and swelling, thus it has better dimensional stability than the *p*-QAPPT counterpart. In comparison, *p*-QAPPT has a lower structural density, and thus exhibits higher swelling and water absorption.

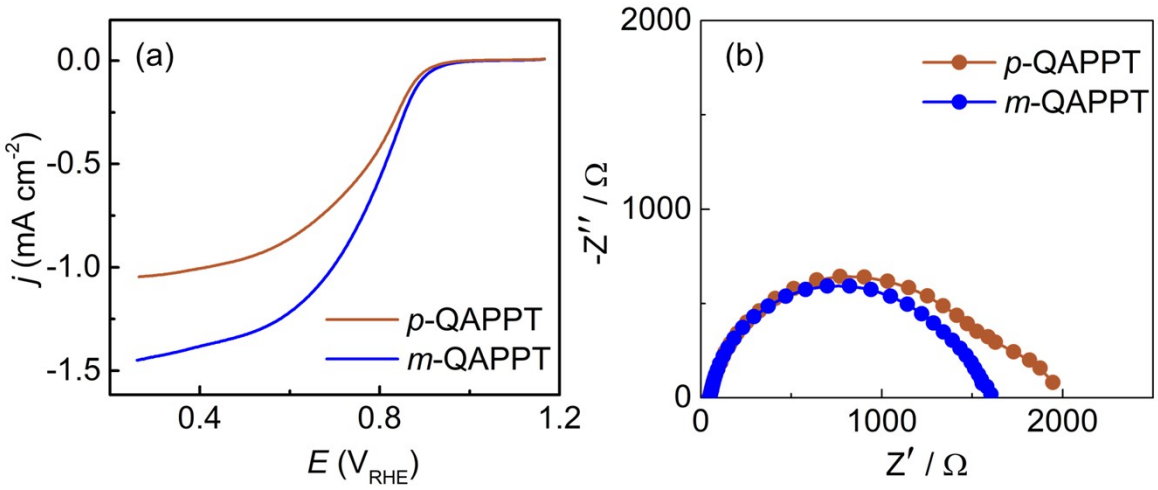

Fig. S2 RDE test on the platinum disk in 0.1 M KOH aqueous electrolyte at 25 °C: (a) Linear scan voltammetry curves at 5 mV s^{-1} at 1600 rpm. (b) Electrochemical impedance spectra at 0.85 V_{RHE}.

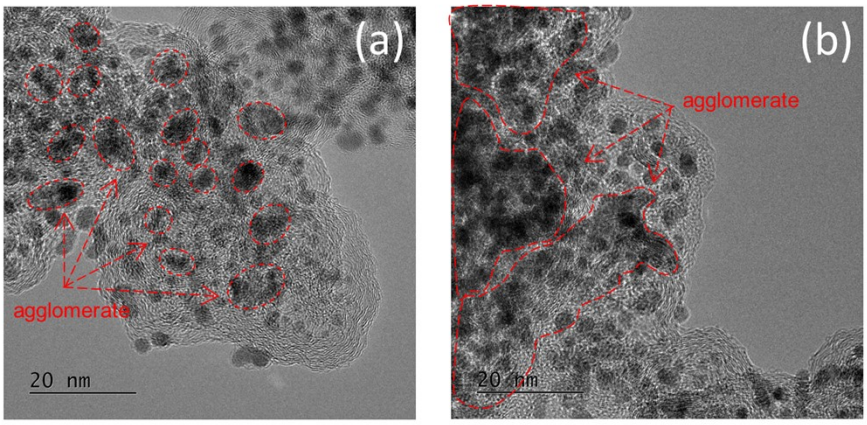

Fig. S3 Typical TEM images of the 60% Pt/C catalyst with different AEIs: (a) *m*-QAPPT. (b) *p*-QAPPT. Catalyst inks: 60% Pt/C dispersed in a mixture of ionomer solution, water and isopropanol.

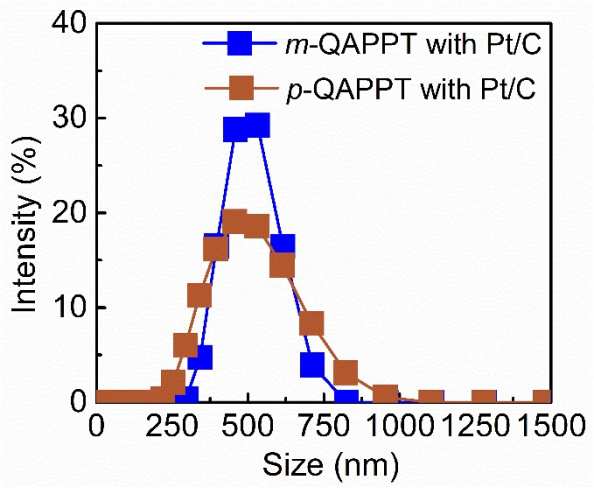

Fig. S4 Agglomerate size of different AEIs with Pt/C catalyst in ethanol solution.

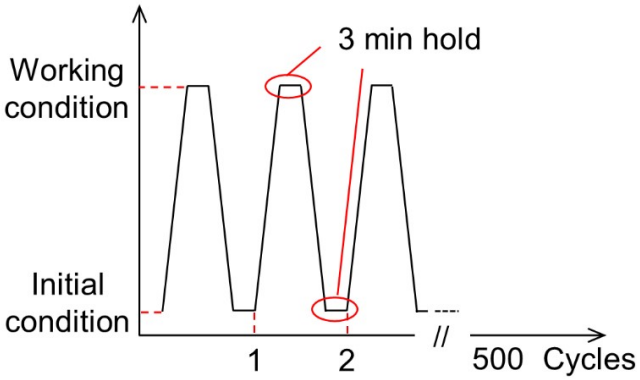

Fig. S5 Scheme for temperature and humidity cycles of accelerated stress tests.

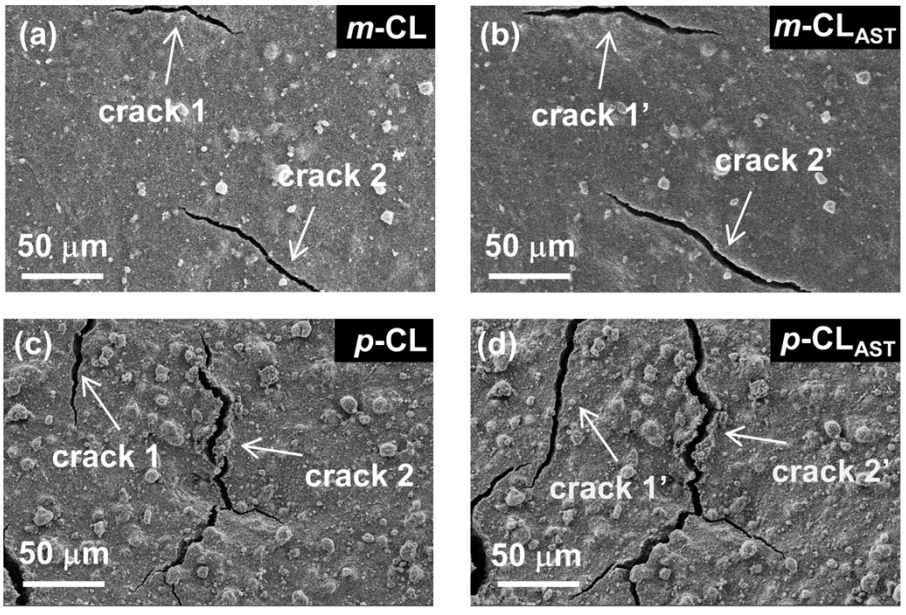

Fig. S6 Topography SEM images of the CLs before (a, c) and after (b, d) ASTs. The increase ratios for the area of crack 1 and crack 2 on *m*-CL (a, b) are 138% and 87%, respectively. The increase ratios for crack 1 and crack 2 on *p*-CL (c, d) are 184% and 142%, respectively.

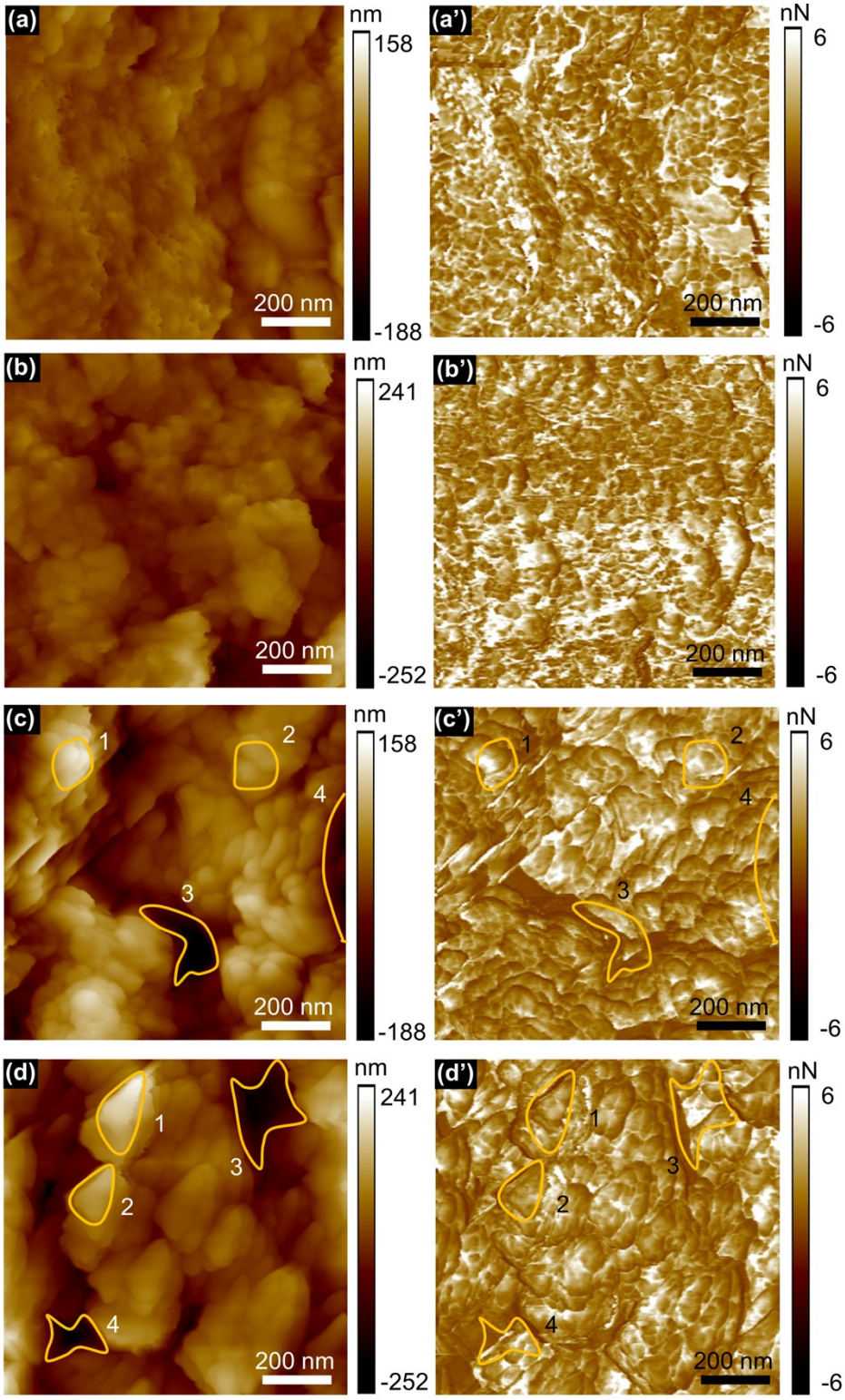

Fig. S7 AFM morphology images (a-d) and corresponding adhesion force mapping (a'−d') images of *m*-CL before (a, a') and after AST (c, c') as well as that of *p*-CL before (b, b') and after AST (d, d'). The regions enclosed by yellow lines represent the high/low positions in AFM images and corresponding ionomer distribution in adhesion force mapping.